Wave Propagation in the Flow of Shear-Thinning Fluids Down an Incline

The effect of shear-thinning rheology on the spatial growth of waves in multilayered flow down an inclined plane is modeled, utilizing the Carreau viscosity constitutive equation. It is shown that waves associated with the free surface propagate as if they were in a Newtonian system, where the viscosity is some average of the varying viscosities in the shear-thinning layer. This averaging is due to the global effects of shear thinning, such as changes in velocity profile and film thicknesses. In contrast, waves that are associated with the interfaces between adjacent fluid layers are largely affected by the local interfacial viscosities; wave propagation is not governed by some average Newtonian viscosity across the layer. It is found that shear-thinning rheology can either increase or decrease the growth of waves associated with a fluid-fluid interface, compared with a purely Newtonian case.

Steven J. Weinstein
Emulsion Coating Technologies
Eastman Kodak Company
Rochester, NY 14652

Introduction

The flow of multiple fluid layers down an incline is a fundamental step in the manufacture of many photographic products. The inclined plane itself provides a means by which individual fluid layers can be stacked on top of one another; at the end of the plane, these layers are deposited simultaneously on a moving substrate. Prescribed layer thicknesses on the substrate are easily obtained by premetering the flow, that is, the flow rate of liquids to the inclined plane and speed of the substrate are controlled. It is well known that the flow down the inclined plane can be unstable. These instabilities manifest themselves as waves that travel along the fluid interfaces, down the inclined plane in the direction of the bulk fluid flow. Unfortunately, the waves formed on the incline can translate onto the substrate, and this can give rise to coating nonuniformities. It is clearly desirable to identify those conditions under which these instabilities occur, so that these conditions can be avoided.

An important feature of the waves, while they are small in amplitude, is that they grow or decay on the incline according to the formula:

$$A_f = A_i \cdot (\text{Gain}) \tag{1a}$$

$$\text{Gain} = e^{\nu W} \tag{1b}$$

where A_f is the final wave amplitude, A_i is the initial wave amplitude, ν is the growth factor, and W is the length of the incline. This formula reflects the fact that spatial growth is exhibited by waves formed on an inclined plane. It is desirable to minimize the final wave amplitude A_f to minimize the coating nonuniformities. The initial disturbance giving rise to the wave determines the size of A_i; unfortunately, the initial wave amplitude is not the amplitude of the specific disturbance that induces the wave to form since not all the energy of a disturbance is transferred to the wave. Consequently, it is necessary either to experimentally or theoretically determine which disturbances and conditions yield the largest values of A_i. The gain (the growth of the wave) is quantified by the exponential given in Eq. 1b, and the growth can be reduced by decreasing both the length of the incline and growth factor. The growth factor, ν, is determined by the specific fluid and flow properties; choosing flow conditions wisely allows for a significant decrease in the growth factor. This paper will specifically focus on the determination of ν in Eq. 1b.

There is an extensive literature on the stability of Newtonian flow down an inclined plane for single-layer systems (Benjamin, 1957; Binnie, 1957; Yih, 1963; and many others). An important characteristic of these studies is that the stability is governed by the Reynolds number, $Re = \rho Q/\eta$ (where ρ is the density, Q, is the volumetric flow rate per unit width, and η is the viscosity), for a given angle of inclination, β, where increasing the Reynolds number beyond a critical value induces instability. Thus, the instability for a Newtonian single layer is induced by the

presence of inertial forces as characterized by the Reynolds number. The single-layer flow down an incline of a non-Newtonian fluid has been much less studied. Yet, it is clear that different non-Newtonian constitutive equations can play a significant role in the system stability (Yih, 1965; Lin, 1967; Shaqfeh et al., 1989).

Multiple-layer Newtonian systems have also been considered. Kao (1965a,b, 1968) investigated the effect of viscosity and density stratification in two-layer systems on the stability of the flow, restricting attention to long wavelengths. Akhtaruzzaman et al. (1978) investigated the long-wavelength motion of a three-layer system, the stability of which was subsequently determined by Wang et al. (1978). Both of these analyses indicate that the number of wave solutions is generally equal to the number of interfaces in the problem. Results by Loewenhurz and Lawrence (1989) demonstrate that inertia is not necessary to induce instability in a two-layer system. The wave solution associated with the free surface (referred to as the surface mode) is stable in the zero Reynolds number limit, in keeping with the single-layer results stated previously. However, the wave solution associated with the fluid–fluid interface (referred to as the interface mode) is shown to be unstable at zero Reynolds number due to a jump in viscosity—in particular, when the top layer viscosity is greater than the bottom layer viscosity. Furthermore, the largest growth of this interface mode occurs at finite wavelengths, and is not accessible in the long-wavelength limit.

Hooper and Boyd (1983) investigated the instability mechanism associated with the interface between two fluids of different viscosities via an energy balance. They found that the cause of the instability is energy that is transferred from the uniform fluid flow to the perturbed linearized equations by the perturbation shear stress along the interface. This term is nonzero whenever there is a viscosity jump across the interface. In the limit of small wavelengths, they demonstrated that the effect of this viscosity jump dominated inertial effects in driving instabilities. Using a similar energy approach, Kelly et al. (1989) investigated the instability mechanism associated with the free surface in a single-layer system, and they identified a similar term to that of Hooper and Boyd (1983) as being responsible for the instability.

Investigations of the effect of shear thinning for multiple layers have focused on confined flows with no free surface. Waters (1983) considered the long-wavelength stability of two-layer Couette flow, where the fluids obeyed a power law dependence in each layer. He found that shear-dependent viscosities have a large effect on the neutral stability of the flow. Waters and Keely (1987) investigated the two-layer Couette flow of Oldroyd liquids, and found that the system stability is not attributable to the effective viscosities of the layer; the way in which the fluid viscosities depend on shear rate is important in determining neutral stability. Results by Anturkar et al. (1990) further demonstrate that the way in which fluids shear thin is important in determining the neutral stability of Poiseuille flow.

All of the literature cited for multiple-layer flow down an incline has been concerned with Newtonian systems. The purpose of this paper is to determine the effect of shear-thinning fluids on the wave growth associated with premetered multiple-layer flow down an inclined plane. To this end, the effect of shear thinning is demonstrated through various comparisons between shear-thinning and Newtonian systems. It is seen that shear-thinning rheology affects the surface mode waves quite differently from the interface mode waves. The previously cited work of Hooper and Boyd (1983) and Kelly et al. (1989) is used to postulate an explanation for the results.

It is important to note here that much of the previous work cited has focused on the determination of neutral stability (i.e., out of all possible waves that can form, the wave having largest growth has $\nu = 0$ in Eq. 1). In coating operations, however, conditions characterizing neutral stability are often not the most useful "stability" criteria, since some wave growth may be tolerated in practice. Consequently, requiring that neutral stability criteria be satisfied can sometimes lead to overrestrictive constraints on processes. Thus, this paper will focus primarily on predictions of wave growth away from conditions near neutral stability.

In the previous work cited above, film thicknesses on the incline are specified and the velocity field and volumetric flows in each layer can subsequently be determined. However, in considering coating processes where flows are premetered, the film thicknesses play a passive role, and are thus *dependent* variables. Thus, in this paper, the flow rates in each layer are specified, and are thus the natural variables to use in constructing dimensionless groups that characterize the system.

Formulation

The Carreau model for the non-Newtonian viscosity (Bird et al., 1977) is used in both the uniform flow and stability calculations to model the shear-thinning behavior of the fluids. For a Newtonian fluid, the stress is related to strain by:

$$\tau = \eta\dot{\gamma} \tag{2a}$$

where τ is the stress tensor, η is the constant Newtonian viscosity, and $\dot{\gamma}$ is the rate of strain tensor. For the Carreau model fluid, the constitutive relation in Eq. 2a is modified, where η is now a function of $|\dot{\gamma}|$, the magnitude of the rate of strain:

$$\frac{\eta - \eta_\infty}{\eta_c - \eta_\infty} = [1 + (\delta|\dot{\gamma}|)^2]^{(n-1)/2} \tag{2b}$$

where for flow in two dimensions:

$$|\dot{\gamma}|^2 = 2\left(\frac{\partial V_x}{\partial x}\right)^2 + 2\left(\frac{\partial V_y}{\partial y}\right)^2 + \left(\frac{\partial V_x}{\partial y} + \frac{\partial V_y}{\partial x}\right)^2 \tag{2c}$$

In Eq. 2b, η_∞ is the viscosity at large strain rates, η_c is the low strain Newtonian viscosity, and δ and n are fitted parameters. This model predicts viscosities that smoothly connect Newtonian behavior at low strain rates with a power law curve at large strain rates. The Newtonian limiting behavior is especially important in modeling the motion of waves on a free surface, since the rate of strain there is zero. If a simple power law model were used, the viscosity would be infinite at the free surface, and realistic predictions of wave motion and growth would probably not be obtained.

Uniform film equations

Several layers of fluids with specified properties are flowing down an infinite plane inclined at angle β, where the volumetric flow rate in each layer is specified, Figure 1. The fluid interfaces

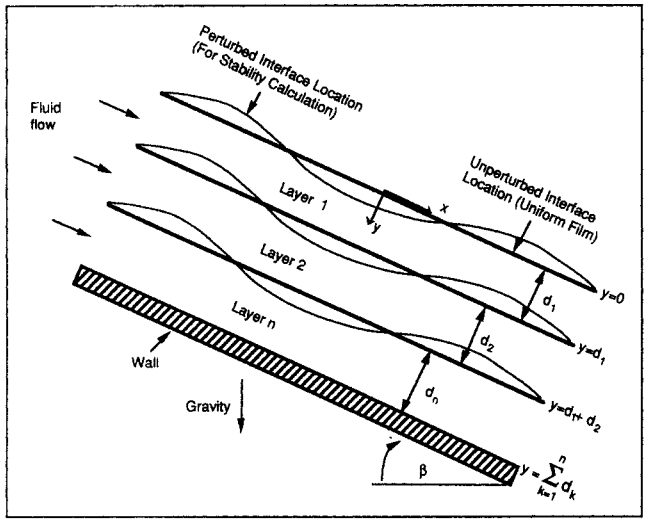

Figure 1. Geometry of uniform film and stability problems.

and free surface are all parallel to the solid inclined surface (hereafter called the wall), and the flow in each layer is everywhere parallel to the wall. The goal is to determine the film thicknesses, velocity field, and rates of strain in each layer. Let the origin of the x–y coordinate system be placed at the free surface, the y axis oriented toward the wall. Denote the top layer of the pack as layer 1, the second as 2, and so on to layer n. All fluid properties, flows, and film thicknesses are denoted with subscript k using this convention.

Since the film thicknesses of each layer are not known *a priori*, it is convenient to manufacture a different length scale that can be used to make all the equations dimensionless. In this way, dimensionless groups are obtained that are independent of these unknown thicknesses. An appropriate length scale, denoted by d_s, is given by:

$$d_s = \left[\frac{\eta_{c_n} Q_T}{\rho_n g \sin\beta}\right]^{1/3} \tag{3}$$

In Eq. 3, Q_T denotes the total flow per unit width of the multiple layer system, ρ is the density, and g is the gravitational constant. Thus, $y \sim d_s$, while the velocity in each layer scales as $V_{x_k} \sim Q_T/d_s$. The viscosity in each layer, η_k, scales with η_{c_n}. It turns out that the pressure in the uniform film problem is hydrostatic, and thus does not interact with the fluid flow. The choice for this pressure scale is made based on dynamics of the stability problem to be considered subsequently; for convenience, the pressure is made dimensionless here as $P_k \sim \rho_n Q_T^2/d_s^2$, and $x \sim d_s$. All dimensionless quantities will be denoted with an overbar.

For uniform parallel flow in each layer, a force balance on the fluid leads to the following governing equations:

$$\frac{d\bar{\tau}_{xy_k}}{d\bar{y}} = Re\frac{\partial \bar{P}_k}{\partial \bar{x}} - M_k \tag{4}$$

$$\frac{\partial \bar{P}_k}{\partial \bar{y}} = \frac{M_k \cot\beta}{Re} \tag{5}$$

where $Re = \rho_n Q_T/\eta_{c_n}$ (a characteristic Reynolds number), $M_k = \rho_k/\rho_n$, and $\bar{\tau}_{xy_k}$ is the only nonzero component of the stress tensor written using Eq. 2:

$$\bar{\tau}_{xy_k} = \bar{\eta}_k \frac{d\bar{V}_{x_k}}{d\bar{y}} \quad k \in [1, n] \tag{6a}$$

and:

$$\bar{\eta}_k = E_k\left\{I_k + (1 - I_k)\left[1 + \left(L_k \frac{d\bar{V}_{x_k}}{d\bar{y}}\right)^2\right]^{(n_k-1)/2}\right\} \tag{6b}$$

In Eq. 6b, $E_k = \eta_{c_k}/\eta_{c_n}$, $I_k = \eta_{\infty_k}/\eta_{c_k}$, and $L_k = \delta_k Q_T/d_s^2$. Denoting the dimensionless thickness of each layer as $\bar{d}_k = d_k/d_s$, the continuity of normal and tangential stress at each interface yields:

$$\left\{\begin{matrix}\bar{\tau}_{xy_k} = \bar{\tau}_{xy_{k-1}} \\ \bar{P}_k = \bar{P}_{k-1}\end{matrix}\right\} \quad \text{at } \bar{y} = \sum_{i=0}^{k-1} \bar{d}_i,\ k \in [1, n] \tag{7a,b}$$

where:

$$\bar{d}_0 = \bar{\tau}_{xy_0} = \bar{\eta}_0 = 0, \text{ and } \bar{P}_0 = \bar{P}_a \tag{7c}$$

In Eq. 7c, $\bar{P}_a$ is the atmospheric pressure. Continuity of velocities across each layer yields:

$$\bar{V}_{x_k} = \bar{V}_{x_{k-1}} \quad \text{at} \quad \bar{y} = \sum_{i=0}^{k-1} \bar{d}_i,\ k \in [2, n] \tag{8}$$

while no-slip at the solid surface gives:

$$\bar{V}_{x_n} = 0 \text{ at } \bar{y} = \sum_{k=0}^{n} \bar{d}_k \tag{9}$$

The final condition constrains the velocity to satisfy the dimensionless volumetric flow rate, $\bar{Q}_k = Q_k/Q_T$, in each layer, that is, $k \in [1, n]$:

$$\bar{Q}_k = \int_{\sum_{i=0}^{k-1} \bar{d}_i}^{\sum_{i=0}^{k} \bar{d}_i} \bar{V}_{x_k}\, d\bar{y} \tag{10}$$

The above equations and the boundary conditions in Eqs. 4 to 10 represent a well-posed boundary-value problem to solve for the velocity field and film thicknesses in each layer. These are now simplified to aid in their numerical solution.

The pressure in each layer is obtained by integrating Eq. 5 using Eq. 7b:

$$\bar{P}_k = \frac{M_k \cot\beta}{Re}\left\{\bar{y} - \sum_{i=1}^{k-1} \bar{d}_i\right\} + \frac{\cot\beta}{Re}\sum_{i=1}^{k-1} M_i \bar{d}_i + \bar{P}_a \tag{11}$$

Equation 4 is integrated once with respect to $\bar{y}$ to obtain:

$$\bar{\tau}_{xy_k} = -M_k \bar{y} + C_k \tag{12a}$$

where the C_k values are obtained by applying Eq. 7a:

$$C_k = \sum_{i=1}^{k} (M_i - M_{i-1}) \sum_{m=0}^{i-1} \bar{d}_m \tag{12b}$$

Equations 6, 8 to 10, and 12 constitute the simplified boundary-value problem to be solved to find the film thicknesses and the flow field. From these equations, it is apparent that:

$$\bar{d}_k = F_k(M_l, \bar{Q}_l, E_l, I_i, L_i, n_i) \qquad i, k \in [1, n], l \in [1, n-1] \tag{13}$$

where F_k is a dimensionless function. It is thus seen that the above choice of d_s allows the explicit removal of the incline angle, β, from the uniform flow problem.

Stability equations

In what follows, the equations used to assess the linear stability of the uniform flow equations are presented; to this end, the same coordinate system is used, Figure 1. All disturbances are assumed to be two-dimensional, that is, uniform across the width of the inclined plane. In addition, it is assumed that the fluid interfaces have surface tensions, σ_k, and that there are no surfactants present there. The amplitude of waves that form on the incline is assumed to be small; thus, wave solutions can be obtained by assuming perturbations about the uniform flow solution discussed in the previous section (here subscripted 0 for clarity) as:

$$\bar{V}_{x_k} \sim \bar{V}_{x_k}(\bar{y})_0 + \tilde{V}_{x_k}(\bar{x}, \bar{y}, \bar{t}) \tag{14a}$$

$$\bar{V}_{y_k} \sim \tilde{V}_{y_k}(\bar{x}, \bar{y}, \bar{t}) \tag{14b}$$

$$\bar{P}_k \sim \bar{P}_k(y)_0 + \tilde{P}_k(\bar{x}, \bar{y}, \bar{t}) \tag{14c}$$

$$\tilde{\zeta}_k \sim \sum_{i=0}^{k-1} \bar{d}_i + \tilde{\zeta}_k(\bar{x}, \bar{t}) \tag{14d}$$

In Eq. 14 a tilde is used to denote the small dimensionless perturbed quantities. The time variable is denoted by $\bar{t}d_s^2/Q_T$, the velocity in the y direction is given by $\bar{V}_{y_k} Q_T/d_s$, and the interface location is given by $\bar{\zeta}_k d_s$.

The expansions, Eqs. 14a–d, are introduced into the governing equations and boundary conditions, and terms quadratic or higher in the perturbed quantities are ignored; that is, a linear approximation is considered. In what follows, the subscript 0 is dropped from the uniform flow results for simplicity; the perturbed and base flow quantities are distinguished only by a tilde and overbar, respectively. The continuity equation becomes:

$$\frac{\partial \tilde{V}_{x_k}}{\partial \bar{x}} + \frac{\partial \tilde{V}_{y_k}}{\partial \bar{y}} = 0 \tag{15}$$

The linearized momentum equations are:

$$M_k Re\left[\frac{\partial \tilde{V}_{x_k}}{\partial \bar{t}} + \bar{V}_{x_k}\frac{\partial \tilde{V}_{x_k}}{\partial \bar{x}} + \tilde{V}_{y_k}\frac{d\bar{V}_{x_k}}{d\bar{y}}\right] = -Re\frac{\partial \tilde{P}_k}{\partial \bar{x}} + \frac{\partial \tilde{\tau}_{xx_k}}{\partial \bar{x}} + \frac{\partial \tilde{\tau}_{xy_k}}{\partial \bar{y}} \tag{16a}$$

$$M_k Re\left[\frac{\partial \tilde{V}_{y_k}}{\partial \bar{t}} + \bar{V}_{x_k}\frac{\partial \tilde{V}_{y_k}}{\partial \bar{x}}\right] = -Re\frac{\partial \tilde{P}_k}{\partial \bar{y}} + \frac{\partial \tilde{\tau}_{xy_k}}{\partial \bar{x}} + \frac{\partial \tilde{\tau}_{yy_k}}{\partial \bar{y}} \tag{16b}$$

where:

$$\tilde{\tau}_{xx_k} = 2\bar{\eta}_k \frac{\partial \tilde{V}_{x_k}}{\partial \bar{x}} \tag{16c}$$

$$\tilde{\tau}_{yy_k} = 2\bar{\eta}_k \frac{\partial \tilde{V}_{y_k}}{\partial \bar{y}} \tag{16d}$$

$$\tilde{\tau}_{xy_k} = \bar{\theta}_k\left[\frac{\partial \tilde{V}_{x_k}}{\partial \bar{y}} + \frac{\partial \tilde{V}_{y_k}}{\partial \bar{x}}\right] \tag{16e}$$

and:

$$\bar{\theta}_k = E_k\left\{I_k + (1 - I_k)\left[1 + n_k\left(L_k\frac{d\bar{V}_{x_k}}{d\bar{y}}\right)^2\right] \cdot \left[1 + \left(L_k\frac{d\bar{V}_{x_k}}{d\bar{y}}\right)^2\right]^{(n_k-3)/2}\right\} \tag{16f}$$

In Eqs. 15 and 16, $k \in [1, n]$, where the definition of $\bar{\eta}_k$ in Eqs. 16c,d is given by Eq. 6b. The no-slip and kinematic boundary conditions at the plate surface become:

$$\begin{pmatrix} \tilde{V}_{x_n} = 0 \\ \tilde{V}_{y_n} = 0 \end{pmatrix} \quad \text{at } \bar{y} = \sum_{k=0}^{n} d_k \tag{17}$$

The kinematic condition at each interface is given by:

$$\tilde{V}_{y_k} = \frac{\partial \tilde{\zeta}_k}{\partial \bar{t}} + \bar{V}_{x_k}\frac{\partial \tilde{\zeta}_k}{\partial \bar{x}} \quad \text{at } \bar{y} = \sum_{i=0}^{k-1} \bar{d}_i,\ k \in [1, n] \tag{18}$$

while the continuity of velocities across each interface is given by:

$$\begin{pmatrix} \tilde{V}_{x_k} = \tilde{V}_{x_{k-1}} + \tilde{\zeta}_k\left[\frac{d\bar{V}_{x_{k-1}}}{d\bar{y}} - \frac{d\bar{V}_{x_k}}{d\bar{y}}\right] \\ \tilde{V}_{y_k} = \tilde{V}_{y_{k-1}} \end{pmatrix} \quad \text{at } \bar{y} = \sum_{i=0}^{k-1} \bar{d}_i,\ k \in [2, n] \tag{19a,b}$$

The normal and tangential components of the dynamic boundary condition are:

$$\tilde{P}_k - \tilde{P}_{k-1} + (M_k - M_{k-1})\frac{\cot\beta}{Re}\tilde{\zeta}_k + \frac{2}{Re}\left[\bar{\eta}_{k-1}\frac{\partial \tilde{V}_{y_{k-1}}}{\partial \bar{y}} - \bar{\eta}_k\frac{\partial \tilde{V}_{y_k}}{\partial \bar{y}}\right] - \frac{1}{ReCa_k}\frac{\partial^2 \tilde{\zeta}_k}{\partial \bar{x}^2} = 0 \quad \text{at } \bar{y} = \sum_{i=0}^{k-1} \bar{d}_i,\ k \in [1, n] \tag{20a}$$

$$\tilde{\tau}_{xy_k} - \tilde{\tau}_{xy_{k-1}} - (M_k - M_{k-1})\tilde{\zeta}_k = 0 \quad \text{at } \bar{y} = \sum_{i=0}^{k-1} \bar{d}_i,\ k \in [1, n] \tag{20b}$$

where $Ca_k = \eta_{c_n} Q_T/\sigma_k d_s$ is a capillary number.

It is convenient to define a stream function, which automatically satisfies Eq. 15 and removes the explicit appearance of the pressure in the above system:

$$\tilde{V}_{x_k} = \frac{\partial \psi_k}{\partial \bar{y}}, \qquad \tilde{V}_{y_k} = -\frac{\partial \psi_k}{\partial \bar{x}} \tag{21}$$

These quantities are substituted into the above equations, and an equivalent boundary-value problem to solve for ψ_k is obtained. All solutions to the above equations can be written as the superposition of traveling waves of the form:

$$\psi_k = R_k(\bar{y}) e^{i(\alpha \bar{x} - \omega \bar{t})} \tag{22a}$$

$$\tilde{\zeta}_k = T_k e^{i(\alpha \bar{x} - \omega \bar{t})} \tag{22b}$$

where it is necessary to determine the unknown functions $R_k(\bar{y})$, the unkown constants T_k, and the functionality $\alpha(\omega)$. In Eqs. 22, i denotes imaginary, $2\pi\omega Q_T/d_s^2$ is the purely real frequency, $\alpha = \alpha_R + i\alpha_I$ is the complex wave number, where the real part of α is defined as $\alpha_R = 2\pi d_s/\lambda$ (λ is the wavelength), and the imaginary part of α, denoted by α_I, determines the spatial growth or decay of waves along the inclined plane.

The assumed forms given in Eqs. 22 are substituted into the above governing equations, Eqs. 15 to 20. The constants T_k are written in terms of R_k at each interface by using the kinematic conditions, Eq. 18:

$$T_k = \frac{\alpha R_k}{(\omega - \alpha \overline{V}_{x_k})}\bigg|_{\bar{y} = \sum_{i=0}^{k-1} \bar{d}_i} \tag{23}$$

The result given by Eq. 23 allows a boundary-value problem to be obtained totally in terms of the unknown R_k functions. A single governing equation for each layer, equivalent to the continuity equation and momentum equations, Eqs. 15 and 16a,b, is given by:

$$\frac{d^2\Theta_k}{d\bar{y}^2} - 4\alpha^2 \frac{d\Phi_k}{d\bar{y}} + \alpha^2 \Theta_k = -iReM_k(\omega - \alpha \overline{V}_{x_k})\left(\frac{d^2R_k}{d\bar{y}^2} - \alpha^2 R_k\right) - i\alpha ReM_k R_k \frac{d^2\overline{V}_{x_k}}{d\bar{y}^2} \tag{24a}$$

where $k \in [1, n]$, and:

$$\Phi_k(\bar{y}) = \bar{\eta}_k \frac{dR_k}{d\bar{y}} \tag{24b}$$

$$\Theta_k(\bar{y}) = \bar{\theta}_k \left[\frac{d^2R_k}{d\bar{y}^2} + \alpha^2 R_k\right] \tag{24c}$$

The no-slip and kinematic conditions, Eq. 17, become:

$$\begin{pmatrix} R_n = 0 \\ \dfrac{dR_n}{d\bar{y}} = 0 \end{pmatrix} \quad \text{at } \bar{y} = \sum_{k=0}^{n} \bar{d}_k \tag{24d,e}$$

while continuity of velocities at each interface, condition Eqs. 19a,b, are rewritten for $k \in [2, n]$ as:

$$\begin{pmatrix} \dfrac{dR_k}{d\bar{y}} = \dfrac{dR_{k-1}}{d\bar{y}} + \dfrac{\alpha R_k}{(\omega - \alpha \overline{V}_{x_k})}\left[\dfrac{d\overline{V}_{x_{k-1}}}{d\bar{y}} - \dfrac{d\overline{V}_{x_k}}{d\bar{y}}\right] \\ R_k = R_{k-1} \end{pmatrix} \quad \text{at } \bar{y} = \sum_{i=0}^{k-1} \bar{d}_i \tag{24f,g}$$

The normal and tangential components of the dynamic boundary conditions, Eqs. 20, become:

$$R_k \left\{ \frac{i\alpha^2}{(\omega - \alpha \overline{V}_{x_k})}\left[(M_k - M_{k-1}) \cot \beta + \frac{\alpha^2}{Ca_k}\right] + i\alpha Re\left[M_k \frac{d\overline{V}_{y_k}}{d\bar{y}} - M_{k-1} \frac{d\overline{V}_{y_{k-1}}}{d\bar{y}}\right]\right\} + \frac{dR_k}{d\bar{y}}[iReM_k(\omega - \alpha \overline{V}_{x_k}) - 2\alpha^2 \bar{\eta}_k] - \frac{dR_{k-1}}{d\bar{y}}[iReM_{k-1}(\omega - \alpha \overline{V}_{x_k}) - 2\alpha^2 \bar{\eta}_{k-1}] - 2\alpha^2[\Phi_k - \Phi_{k-1}] + \left[\frac{d\Theta_k}{d\bar{y}} - \frac{d\Theta_{k-1}}{d\bar{y}}\right] = 0 \quad \text{at } \bar{y} = \sum_{i=0}^{k-1} \bar{d}_i,\ k \in [1, n] \tag{24h}$$

$$\Theta_k - \Theta_{k-1} - (M_k - M_{k-1}) \frac{\alpha R_k}{(\omega - \alpha \overline{V}_{x_k})} = 0 \quad \text{at } \bar{y} = \sum_{i=0}^{k-1} \bar{d}_i,\ k \in [1, n] \tag{24i}$$

The boundary-value problem, Eqs. 24, constitutes a homogeneous system of equations and boundary conditions, that is, a nonlinear eigenvalue problem to determine the complex number α as a function of ω for given physical, geometrical, and flow properties as:

$$\alpha = G(M_l, \overline{Q}_l, E_l, I_i, L_i, n_i, Re, \omega, Ca_i, \cot \beta) \qquad i \in [1, n],\ l \in [1, n-1] \tag{25}$$

Corresponding complex eigenfunctions are given by Eqs. 22. In general, a specific disturbance to the fluids on the inclined plane excites many individual wave solutions to the system of Eqs. 24, each at a different frequency. However, to assess whether one flow condition is inherently better than another, it suffices to determine how each solution to the above system grows or decays in frequency ranges of practical interest.

Solution Procedure

Uniform film problem

In this section, the numerical solution of the uniform film equations is discussed. The goal is to determine the film thicknesses and velocity profiles in each layer, that is, find $\bar{d}_k$ and $\overline{V}_{x_k}$ for $k \in [1, n]$. The well-posed problem to be solved is given by Eqs. 6, 8–10, and 12.

Since the film thicknesses are not known *a priori*, the domain on which the equations are to be solved is not known. Consequently, the following variable transformation is used to map the unknown interface positions to a known location:

$$Y = 1 - \frac{1}{\bar{d}_k}\left[\bar{y} - \sum_{i=1}^{k-1} \bar{d}_i\right] \qquad k \in [1, n] \tag{26}$$

With this transformation, each layer has a domain of $Y \in [0, 1]$, where $Y = 0$ corresponds to the bounding interface (or wall, for the nth layer) closest to the inclined plane for that layer, and $Y = 1$ corresponds to the upper bounding interface. Thus, all the unknown $\bar{d}_k$ values are incorporated into the governing equations themselves.

A finite difference approximation scheme is used to convert the differential equation system into a set of algebraic equations. The system to be solved is of initial-value form; information that the fluid is not slipping along the wall propagates into the fluid toward the free surface. Each domain, $Y \in [0, 1]$, is discretized into N equal segments, where the velocities are discretized as $\bar{V}_{x_{k,i}}$ with $i \in [0,N]$, and $\bar{V}_{x_{k,0}}$ corresponds to $Y = 0$, while $\bar{V}_{x_{k,N}}$ corresponds to $Y = 1$. To take advantage of the accuracy inherent in using central differences, the discretized Y values used are:

$$Y_k = \frac{k}{N} - \frac{1}{2N} \qquad k \in [1, N] \tag{27}$$

An iterative procedure is employed to determine the film thicknesses and velocities in each layer. First, an initial guess is made for the film thicknesses based upon the Newtonian properties of the system. In dimensional form, the guesses are as in Eq. 28. (The well-known expression for the thickness of a single-layer Newtonian film on an inclined plane is given by $d_1 = \sqrt[3]{3\bar{d}_s}$. It is thus seen that the guesses are fractions of an approximate single-layer film thickness, obtained by weighting fluid properties and flow rates.)

$$d_k = \frac{Q_k}{Q_T}\left[\frac{3Q_T}{gB\sin\beta}\right]^{1/3}, \qquad B = \sum_{k=0}^{n} \frac{\rho_k Q_k}{\eta_{c_k} Q_T} \tag{28}$$

Then, the discretized versions of Eqs. 6, 8, 9, and 12 are solved in the following way. Starting at the solid surface, where $\bar{V}_{x_{n,0}} = 0$, the value of Y is incremented to its first value, Y_1, and a nonlinear equation to solve for $\bar{V}_{x_{n,1}}$ is obtained. Newton's method is then employed to find this value, using $\bar{V}_{x_{n,0}}$ as an initial guess. After convergence, Y is incremented to its next value, Y_2, and a nonlinear equation to solve for $\bar{V}_{x_{n,2}}$ is obtained, now using the result for $\bar{V}_{x_{n,1}}$ as an initial guess in Newton's method. This procedure is repeated through each layer and all the way to the free surface, where finally $\bar{V}_{x_{1,N}}$ is determined. Next, the volumetric flow conditions, Eq. 10, are checked, and if satisfied, the film thicknesses and velocity profile obtained are the problem solution. Otherwise, the film thicknesses are updated using Newton's method applied to Eq. 10, where Eq. 10 is interpreted as being only a function of the film thicknesses. The new velocities in each layer are then determined based on these updated film thicknesses as stated above, where the procedure is repeated until the film thicknesses do not change from iteration to iteration to within a desired tolerance.

In addition to the velocities and film thicknesses, it is necessary to determine the rate of strain in each layer, that is, $d\bar{V}_{x_{k,i}}/dY$, for $k \in [1, n]$ and $i \in [0, N]$. Not only are these values of physical interest, but they are necessary in evaluating the stability of the system, as can be seen by inspection of Eq. 24. The finite difference approximation is adequate to determine these derivatives at interior positions of each layer. However, this is not the case at each interface, where $d\bar{V}_{x_{k,N}}/dY$ and $d\bar{V}_{x_{k-1,0}}/dY$ are evaluated. To retain accuracy, the system of Eqs. 6, 8–9, and 12 is solved without finite differencing (where the film thicknesses are already known, and the $d\bar{V}_{x_{k,i}}/dY$ themselves are treated as unknowns instead of the $\bar{V}_{x_{k,i}}$ values), to find the rate of strain values in each layer. Thus, accuracy is obtained at each interface, and in addition, a self-consistency check on the finite difference approximation used to calculate the velocities is obtained.

As a further check on the numerical calculations, an asymptotic solution valid for small shear-thinning effects has been obtained for a single-layer system. The details of this calculation are presented in the appendix. The results are:

$$\bar{V}_x \sim \frac{1}{2}(a^2 - \bar{y}^2) + \frac{L^2}{8}[(1-n)(1-I)(a^4 - \bar{y}^4) + ab] + O(L^4) \text{ as } L \to 0 \tag{29a}$$

$$\bar{d} \sim a + L^2 b \qquad \text{as } L \to 0 \tag{29b}$$

where

$$a = \sqrt[3]{3}, \qquad b = -\tfrac{3}{10}[(1-n)(1-I)] \tag{29c}$$

and all other notation items are as defined previously, except that subscripts denoting the single layer have been omitted.

Stability problem

The numerical procedure used to solve stability Eqs. 24 is now presented. The goal is to determine the complex functionality $\alpha = \alpha(\omega)$, as well as R_k, the complex $\bar{y}$-dependent part of the eigenfunctions. A finite difference approximation is used to approximate all derivatives and thus obtain a set of algebraic equations. In contrast to the uniform film problem, the domain on which the equations are to be solved is known *a priori* (from the solution to the uniform flow problem). Despite this fact, it is convenient to utilize the variable transformation, Eq. 26, to aid in the discretization of the domain. The domain is discretized into N segments as in the uniform film problem using Eq. 27, and functions R_k are discretized as $R_{k,i}$, where $k \in [1, n]$ and $i \in [-2, N + 2]$. The additional $R_{k,i}$ values for $i = -2, -1, N + 1$, and $N + 2$ are values of the functions in an artificially extended domain beyond the particular layer; this discretization allows a central difference quotient to be employed even at the domain boundaries, avoiding errors inherent in a forward difference quotient one might use there. Note that to utilize this discretization, it is also necessary to determine $d\bar{V}_{x_{k,i}}/dY$ (using the procedure outlined in the numerical solution to the uniform film problem) for $i = -1, N + 1$.

Thus, the complex $R_{k,i}$ and α values contribute $n(N + 5) + 1$ unknowns to be determined. Discretized Eq. 24a supplies $n(N + 1)$ equations, Eqs. 24d,e provide two equations, and Eqs. 24h,i provide $2n$ equations. These constitute all the available

equations for a single-layer system. For $n > 1$, $2n - 2$ additional equations are contributed by Eqs. 24f,g. There is one additional equation needed, which is expected because of the singular nature of an eigenvalue system; without loss of generality, the value of $R_{1,N}$ is specified, giving $n(N + 5) + 1$ algebraic equations in $n(N + 5) + 1$ unknowns. Thus, once ω, physical, and geometrical properties are specified, a well-posed system exists to solve for α and the $R_{k,i}$ values.

The discretized system of algebraic equations constitutes a nonlinear eigenvalue problem, and it is thus necessary to employ an iterative procedure to obtain a solution. It is known from existing asymptotic work in the literature (Kao, 1965; Akhtaruzzaman et al., 1978) that there are at most n physical values of α and associated eigenvectors. (There will be fewer than n physical eigensolutions if physical properties are identical in adjacent layers and there is no surface tension between the layers. In this case, by adding the flow rates in each layer there is an identical physical system with $n - 1$ layers, thus accounting for the smaller number of eigensolutions.) Thus, there are multiple solutions to the boundary-value problem, and appropriate initial guesses are needed for each of these solutions. To this end, the long-wavelength approximation is used in the system of Eqs. 24, that is, the limit as $\alpha \to 0$ is taken holding α/ω fixed, retaining terms to $O(\alpha)$. (This limit implies that the wave speed is finite and nonzero at long wavelengths.) This limit linearizes the eigenvalue problem, which subsequently can be solved numerically using conventional techniques. This never fails to provide an initial guess for all solutions to the full eigensystem. [There will be as many eigenvalues as the dimension of the $n(N + 5) + 1$ square matrix. Most of them are readily identified as being artifacts of the discretization. However, solutions that correspond to $(\omega - \alpha \overline{V}_{x_i}) = 0$ can arise, where $\overline{V}_{x_i}$ is the uniform flow velocity at the interface. These must be discarded as well, since they give rise to infinite amplitude interface waves as can be seen in Eq. 23. Note that shear eigenmodes are not accessible in the long-wavelength limit taken.] In addition to this, the long-wavelength approximation results provide a self-consistency check on the solution to the full set of equations.

Newton's method is performed on the system of unknown $R_{k,i}$ values, augmented with α, in the following way. Starting with one of the n (at most) long-wavelength eigensolutions, the frequency is incremented and the full set of equations iterates until a solution is obtained. This procedure is performed for each of the initial long-wavelength eigensolutions. Then the frequency is incremented again, this time using the previously converged solutions as initial guesses for each solution at the new frequency. In this way it is possible to track along each solution branch over the desired frequency range.

Each eigensolution at a given frequency yields a wave solution for each interface. For example, in a two-layer system, at each frequency there are two wavelengths associated with each interface. Rewriting Eq. 1b using the above notation, the total amount that a given wave grows as it moves down the inclined plane, the so-called gain, is given by:

$$\text{Gain}_j = \exp\left[(-\alpha_I)_j \overline{W}\right] \qquad j \le n \tag{30}$$

In Eq. 30, the subscript j denotes the particular eigenvalue whose gain is to be calculated, $\overline{W}d_s$ is the total length of the wall, and $-\alpha_I$ is the dimensionless spatial growth factor.

Results

To check results of the uniform film problem, numerical results were compared with the single-layer asymptotic solution given by Eqs. 29, and the results were in excellent agreement. To check results for multiple fluid layers, Newtonian cases were investigated and the results were compared with analytic parabolic profiles; the results agreed exactly. One further check on the accuracy of the uniform film numerical results was performed by comparing the finite difference and the "exact" strain rates (those strain rates calculated without finite differencing, as discussed in the numerical solution section) at each discretized point in the fluid; typical results deviated by no more than 0.1% at $N = 10$, and were identical to four significant figures for $N \ge 20$. Note also that for the case of $N = 50$, the total run time on an IBM 3090 mainframe computer was less than 1 CPU second for all cases considered. A discretization of $N = 50$ typically gave accuracy to four significant figures in Newtonian uniform film calculations, but it should be noted that for $N = 10$, errors were incurred of no more than 0.5% for all cases examined. Typically, for non-Newtonian cases, the number of grid points must be increased beyond $N = 10$ to achieve the desired accuracy. This is especially true when considering fluids that shear thin considerably in the top layer, since this typically gives rise to rapid variations in the viscosity in the vicinity of the free surface, Figure 2c. It is thus necessary to increase grid points to achieve an adequate approximation for these cases.

For all Newtonian cases, stability results were obtained with $N = 10$, where errors for all cases surveyed were no larger than 1%. This discretization allowed for a reasonable trade-off between run time and accuracy. Run times varied depending upon the frequency increment chosen; typical run times were on the order of 100 CPU seconds. In keeping with the uniform film results for non-Newtonian cases, when a non-Newtonian fluid was in the top layer the number of grid points typically needed to be increased. A check on the numerical stability results was made by comparing them with published results in the literature for Newtonian systems (Yih, 1963; Akhtaruzzaman et al. 1978).

Comparison between Newtonian and shear-thinning cases

In order to assess the effect of shear thinning on the stability of the flow, it is useful to compare with specific Newtonian cases. The choice of these Newtonian cases is considered in what follows. We begin by noting that there are two viscosities that characterize the shear thinning for a given layer, and these are the minimum and maximum viscosities attained in the shear-thinning layer. For example, for a single-layer system, the minimum viscosity attained is the viscosity at the wall, and the maximum is the viscosity at the free surface. Let two Newtonian cases be constructed, one in which the shear-thinning layer is replaced by the minimum viscosity attained (henceforth called the minimum Newtonian case), and the other in which the layer is replaced by the maximum viscosity (henceforth called the maximum Newtonian case) attained. Now, assess the stability of the shear-thinning, minimum Newtonian, and maximum Newtonian systems. If the shear-thinning wave growth is bounded by the two Newtonian cases, then it is concluded that the effect of shear thinning is to provide an averaging effect of

the viscosities across the layer. If not, then some other behavior peculiar to shear thinning is occurring.

The validity of the above comparisons is now discussed from a dimensional analysis point of view. For a single-layer shear-thinning system, Eqs. 13 and 25 become:

$$\bar{d}_1 = F(I_1, L_1, n_1) \tag{31a}$$

$$\alpha = G(I_1, L_1, n_1, Re, \omega, Ca_1, \cot\beta) \tag{31b}$$

In Eq. 31a the parameters I_1, L_1, and n_1 all act to affect viscosities through Eq. 6b. Then, using the above physical arguments it is reasonable to replace these parameters with an effective Newtonian viscosity of either $\bar{\eta}_{1_{min}}$ or $\bar{\eta}_{1_{max}}$, corresponding to the minimum and maximum viscosities in the shear-thinning layer as described above, where these are written using Eq. 6b as:

$$\bar{\eta}_{1_{min}} = I_1 + (1 - I_1)\left[1 + \left(L_1 \frac{d\bar{V}_{x_1}}{d\bar{y}}\right)^2\right]^{(n_1-1)/2} \qquad \bar{y} = \bar{d}_1 \tag{32a}$$

$$\bar{\eta}_{1_{max}} = 1 \tag{32b}$$

Note that in Eqs. 32 the viscosities are made dimensionless with the low-strain Newtonian viscosity of the shear-thinning case, that is, η_{c_1}. Then, Eqs. 31 become, for the two Newtonian cases:

$$\bar{d}_1 = F(E) \tag{33a}$$

$$\alpha = G(E, Re, \omega, Ca_1, \cot\beta) \tag{33b}$$

where $E = \bar{\eta}_{1_{min}}$ or $\bar{\eta}_{1_{max}}$.

Then, the comparison between the shear-thinning system, Eqs. 31, and the Newtonian cases, Eqs. 33, is reasonable via dimensional analysis. It should be noted that the film thicknesses will not be the same in the comparison of these cases; this is a consequence of the requirement in this paper that the flow is premetered, and so flow rates are controlled, not film thicknesses. Note also that the above arguments are easily generalized to multiple-layer systems, and so they will not be explicitly presented for these cases.

Using the above arguments, results that elucidate differences between Newtonian and shear-thinning behaviors are presented in what follows. Consider the effect of shear thinning on the flow of a single layer of fluid down an incline. Figures 2a and 2b give the uniform film velocity field and strain rates, while Figure 2c shows a tenfold variation in the viscosity due to the shear-thinning behavior, according to Eq. 6b. In these figures, note that $\bar{d}_T$ is the film thickness of the layer (when multiple layers are considered in what follows, $\bar{d}_T$ is the total film thickness of the multiple-layer system). For purposes of understanding the behavior due to the non-Newtonian fluid, the two Newtonian cases discussed previously are also superimposed on Figures 2a and 2b. The first plotted Newtonian results use the viscosity at the free surface, that is, the Newtonian limit at low strain rates. This is the maximum viscosity the fluid can attain in the fluid layer. The second Newtonian case uses the minimum viscosity the fluid can have in the fluid layer, Figure 2c, that is, the viscosity at the maximum rate of strain at the plate surface. In Figure 2a, the short horizontal lines indicate the position of the

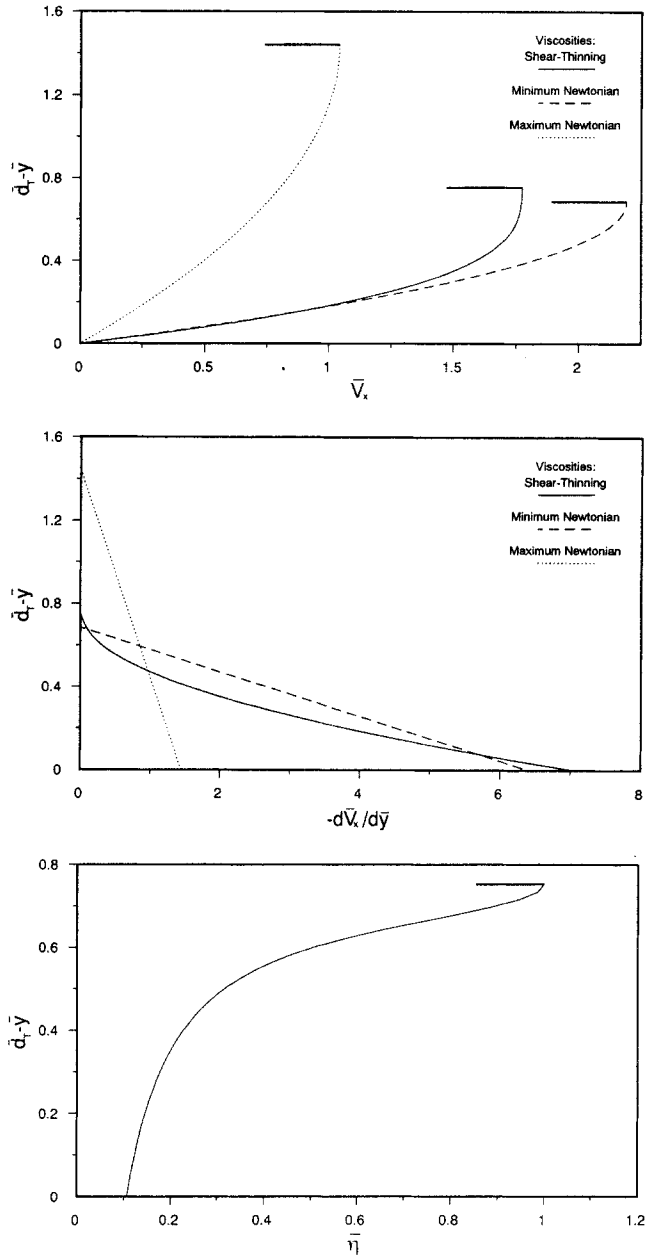

Figure 2. Effect of shear thinning on single layer.
a. *Uniform film velocities*
b. *Rates of strain*
c. *Viscosity*
Conditions: $\beta = 30°$, $Re = 1.00$, $I_1 = 0$, $L_1 = 12.43$, $n_1 = 0.5$, $Ca_1^{-1} = 3.81$
Min. Newtonian viscosity: $\bar{\eta}_{1_{min}} = 0.1068$
Max. Newtonian viscosity: $\bar{\eta}_{1_{max}} = 1.0$

free surface. As one might expect, shear-thinning velocities are larger and the film thickness is smaller than those associated with a Newtonian fluid having the maximum viscosity in the layer; shear-thinning velocities are smaller and the film thickness is larger than those for the case of a corresponding Newtonian fluid with the minimum layer viscosity. The rate of strain at the wall for the shear-thinning case is larger than those for both Newtonian cases, Figure 2b.

Figure 3a gives a plot of the growth factor, $-\alpha_I$, as a function of the frequency, ω, for the non-Newtonian and two Newtonian

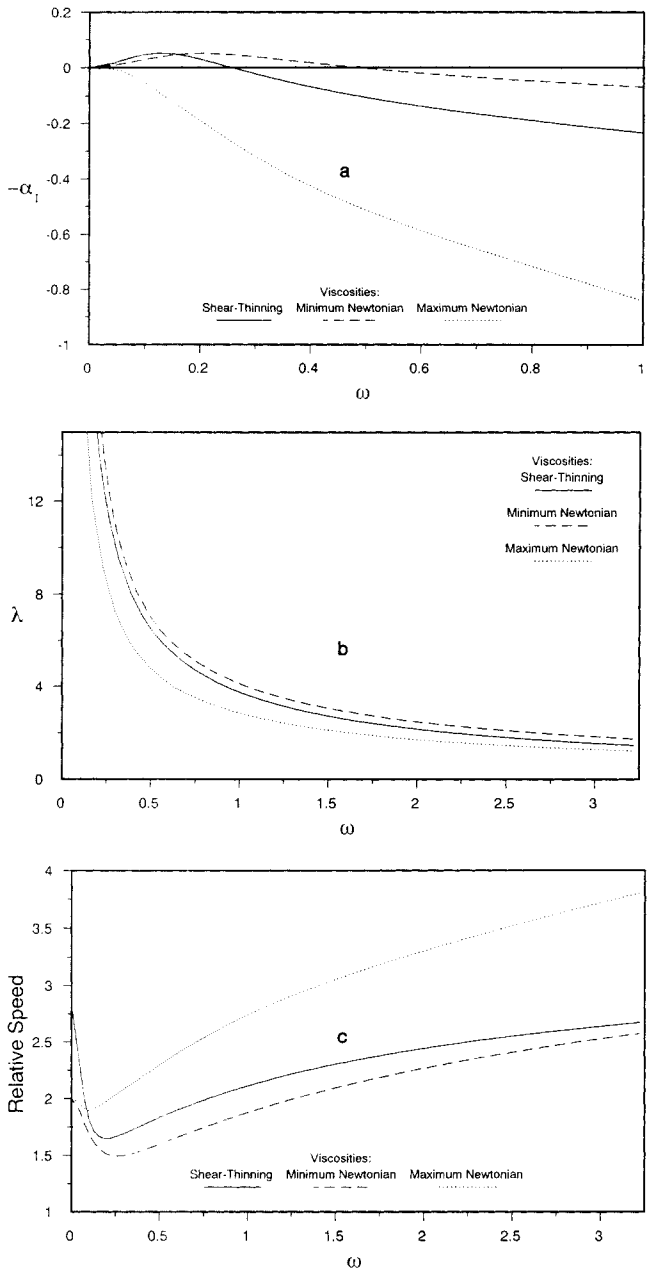

Figure 3. Effect of shear thinning on wave propagation in single-layer flow, corresponding to data of Figure 2.

a. *Growth factors*
b. *Wavelengths*
c. *Wave speeds*

cases previously described. Recall that when $-\alpha_I > 0$, waves of a given frequency are unstable (the line $-\alpha_I = 0$ has been superimposed on Figure 3a and in all growth-factor figures to follow). Figure 3a indicates that the shear-thinning growth factors, corresponding to frequencies of less than approximately 0.15, are slightly larger than for either of the Newtonian cases. Beyond this frequency region, the shear-thinning effects are bracketed by the corresponding minimum and maximum Newtonian viscosity results, the minimum Newtonian viscosity having the largest growth factors. Figure 3b gives a plot of wavelength vs. frequency while Figure 3c gives results for the speed of the surface wave relative to the uniform surface flow. In Figures 3b and 3c, note again that the shear-thinning results lie between the two Newtonian cases except at very low frequencies. Figure 3c indicates that both Newtonian cases limit to relative wave speeds of 2, in agreement with asymptotic theory (Benjamin, 1957), while the shear-thinning case limits to an asymptotic relative speed greater than 2. The degree of shear-thinning behavior determines this deviation from the Newtonian limit. The propagation characteristics (wavelengths, wave speeds, and wave growths) discussed above have been observed for all single-layer cases surveyed.

To further emphasize the single-layer wave growth characteristics, Figure 4 shows growth factors for a case where the shear-thinning viscosities vary to a smaller extent across the layer (approximately a factor of 2). Again, at low frequencies the shear-thinning case is slightly more unstable than either Newtonian case considered. Note that with smaller viscosity variations, the minimum and maximum Newtonian cases become much tighter bounds on the wave growth in the shear-thinning system for higher frequencies.

In considering two-layer systems, results in this paper are given for the case where Ca_2^{-1} is chosen to be zero. This is to match the behavior of typical layers in the photographic industry, where the miscibility of the layers leads to interfaces with no surface tension. Furthermore, for all cases considered, the densities in each layer are taken to be equal, that is, $M_1 = 1$. Consider a two-layer system in which the bottom layer is shear thinning, and the top layer is Newtonian. Figures 5a and 5b show typical uniform film velocity and rate of strain results for the non-Newtonian case, while Figure 5c gives an expanded view of the low rate of strain region shown in Figure 5b. Figure 5d gives the variation of the viscosity in the bottom layer (the viscosity varies by approximately a factor of 4). Also superimposed are two additional Newtonian cases corresponding to the minimum bottom layer viscosity attained at the wall and the maximum bottom layer viscosity at the fluid–fluid interface (hereafter called the interface). For these cases, the top layer conditions are identical to those of the shear-thinning case. In Figure 5a, the short horizontal dotted lines denote the position of

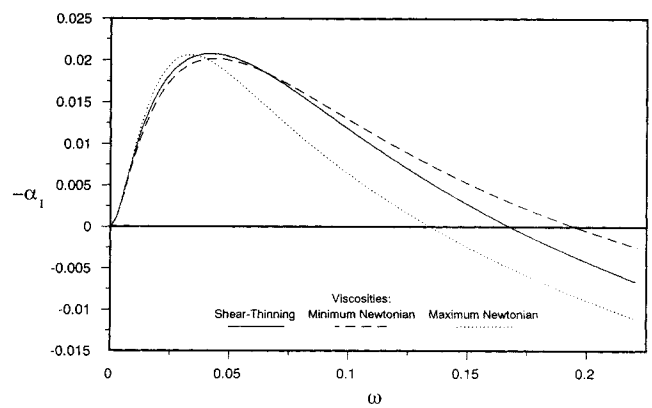

Figure 4. Effect of shear thinning on wave growth in single-layer flow.

Conditions: $\beta = 30°$, $Re = 32.89$, $I_1 = 0$, $L_1 = 6.381$, $n_1 = 0.80$, $Ca_1^{-1} = 39.07$
Min. Newtonian viscosity: $\bar{\eta}_{1_{min}} = 0.5951$
Max. Newtonian viscosity: $\bar{\eta}_{1_{max}} = 1.0$

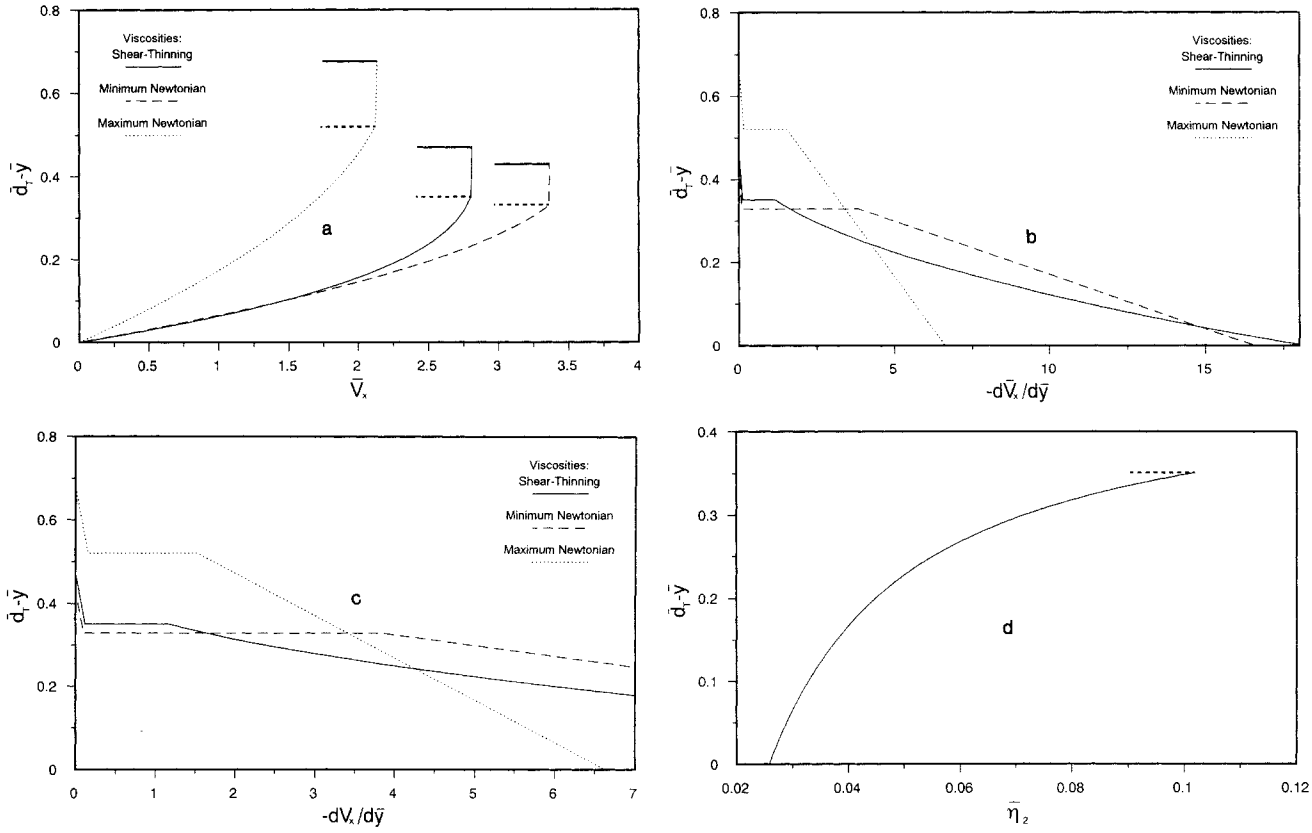

Figure 5. Effect of a shear-thinning bottom layer in a two-layer slide flow.

a. *Uniform film velocities*

b, c. *Rates of strain*

d. *Bottom layer viscosity*

Conditions: $\beta = 30°$, $Re = 15$, $\bar{Q}_1 = 0.33$, $Ca_1^{-1} = 0.84$
Newtonian top layer with $E_1 = 1$
Bottom layer rheology: $I_2 = 0$, $L_2 = 82.56$, $n_2 = 0.5$
Min. Newtonian viscosity: $\bar{\eta}_{2_{min}} = 0.02579$
Max. Newtonian viscosity: $\bar{\eta}_{2_{max}} = 0.1021$

the interlayer, while the short solid lines above them denote the free surface location. Note that shear-thinning film thicknesses of each layer are larger than those associated with the minimum Newtonian viscosity case and are smaller than those for the maximum Newtonian viscosity case; the opposite is true for the velocities. Corresponding rates of strain are shown in Figures 5b and 5c, where the non-Newtonian case is seen to have the largest rate of strain at the wall. Note that in Figures 5b and 5c, the horizontal lines denote the position of the interface, where there is a jump in the rate of strain. Numerical values for the layer thicknesses and the jump in the rate of strain across the interface, for this case and all cases to follow, are given in Table 1 (note that $\Delta S_{\text{interface}}$ in this table denotes the magnitude of the jump in rate of strain across the interface).

There are two wave solutions that arise upon solving this two-layer non-Newtonian system, both traveling along each interface. Figures 6a to 6c give results for the first wave solution. Note that these results have the same trends as for the single-layer results of Figures 3 and 4; for this reason, this solution is denoted as the surface mode. (In fact, it is straightforward to show that the surface mode persists in the limit as the fluid properties become equal in each layer.) Also plotted are the corresponding results for the maximum and minimum Newtonian bottom layer viscosities in the shear-thinning layer. Figures 7a to 7c show the effect of the shear-thinning bottom layer on the second wave solution, which is denoted as the interface mode. Note that these curves are qualitatively different from the surface mode results of Figures 6a to 6c. In the limit as $\omega \to \infty$, the relative wave speed of the interface mode to

Table 1. Film Thicknesses and Jump in Rate of Strain Across Interface

Figure	Viscosity	$\bar{d}_1$	$\bar{d}_2$	$\Delta S_{\text{interface}}$
5,6,7	Shear-thinning	0.1187	0.3510	1.044
	Min. Newtonian	0.09913	0.3287	3.745
	Max. Newtonian	0.1564	0.5201	1.377
8	Shear-thinning	0.3655	0.3102	2.597
	Min. Newtonian	0.3281	0.2997	4.448
	Max. Newtonian	0.4005	0.3684	2.846
	Newtonian limit	0.7368	0.7368	0.3954
9	Shear-thinning	0.4190	0.2299	1.263
	Min. Newtonian	0.3960	0.2224	3.280
	Max. Newtonian	0.4356	0.2614	1.314
	Newtonian limit	0.5945	0.6283	3.317
10	Shear-thinning	1.348	0.3553	1.007
	Min. Newtonian	1.318	0.3585	0.9842
	Max. Newtonian	1.457	0.3444	1.340
11	Shear-thinning	0.2387	0.3764	1.446
	Interface viscosity	0.2808	0.4914	1.701

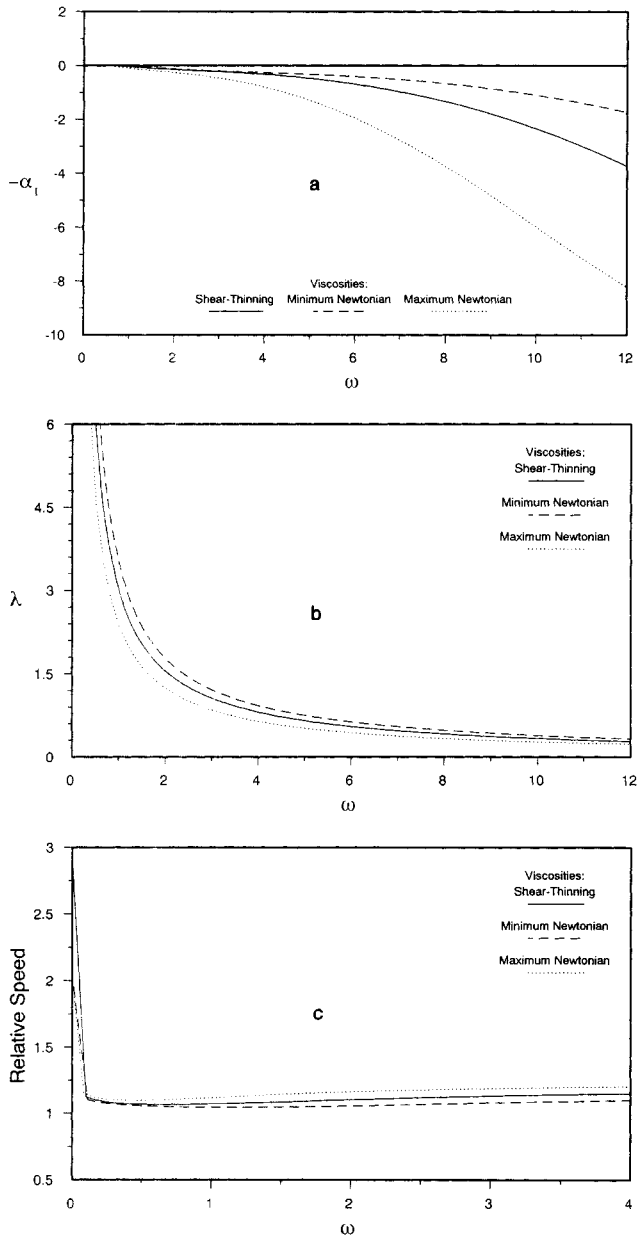

Figure 6. Effect of a shear-thinning bottom layer on surface mode waves in two-layer slide flow for conditions of Fig. 5.

a. *Growth factors*

b. *Wavelengths*

c. *Wave speeds*

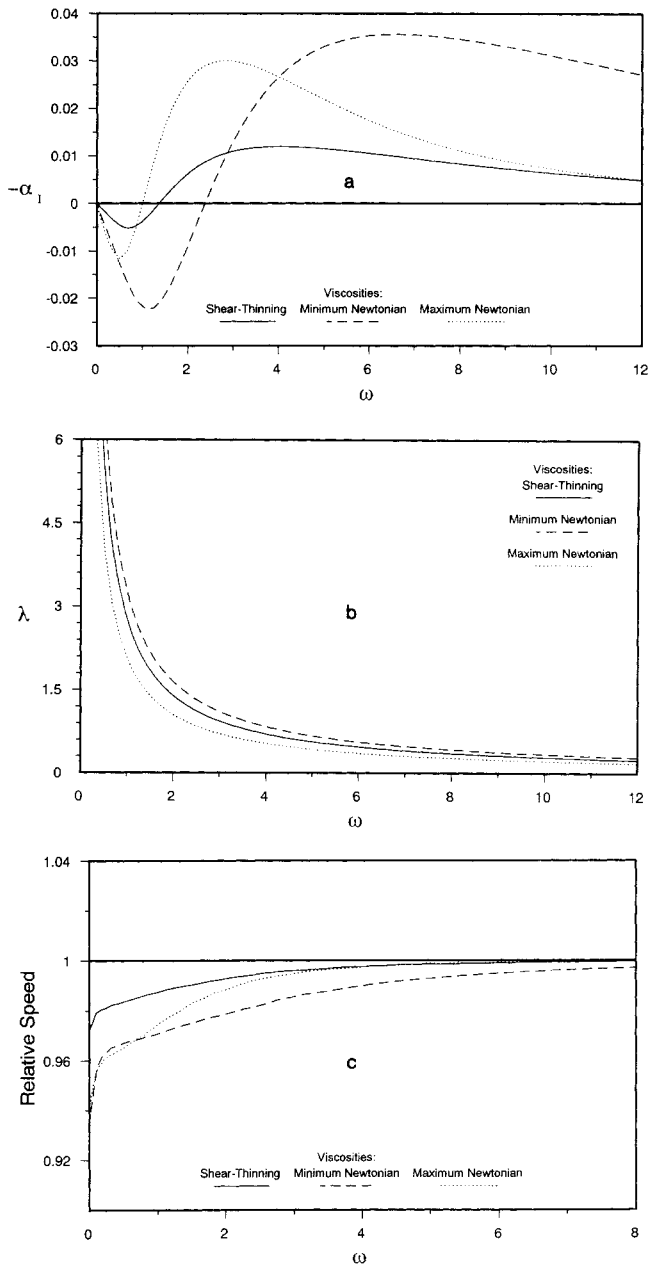

Figure 7. Effect of a shear-thinning bottom layer on interface mode waves in two-layer slide flow for conditions of Fig. 5.

a. *Growth factors*

b. *Wavelengths*

c. *Wave speeds*

the interface uniform velocity appears to asymptote to 1, Figure 7c. (Numerical results were also obtained where the interface mode waves had speeds relative to the interface of greater than 1. It appeared that these cases were limited to those with a lower viscosity upper layer than bottom layer. In all cases surveyed, the interface wave speed approached that of the interface as $\omega \rightarrow \infty$.) This is in contrast to the surface mode results, where the surface mode speeds were always greater than those of the free surface.

Figure 7a indicates the dependence of the interface-mode growth factors on frequency. The maximum growth factors occur at higher frequencies, smaller wavelengths, and exhibit larger growth than those for the surface waves shown in Figure 6a. Further, notice that the non-Newtonian curve no longer lies between the curves corresponding to the maximum and minimum Newtonian viscosities in the bottom layer. Thus, shear-thinning effects lead to maximum wave growth that is smaller than that associated with the corresponding Newtonian cases, which might have been expected to bracket the shear-thinning behavior. At higher frequencies, note that the growth factors associated with the maximum Newtonian case follow quite closely those for the shear-thinning case. For more moderate

frequencies (in the vicinity of $\omega = 2$), there are significant differences in growth factors between these two cases. Note that a least upper bound on the shear-thinning growth factors associated with the interface appears to be given by that of the maximum Newtonian viscosity, that is, the viscosity found in the bottom layer in the vicinity of the interface.

Figures 8a and 8b give growth-factor results for the surface and interface modes, respectively, where more moderate shear thinning occurs in the bottom layer (the viscosity varies by approximately a factor of 2), and the top layer is Newtonian. In Figure 8a, note as before that the shear-thinning results lie between those for the maximum and minimum Newtonian cases. Figure 8b shows that the interface mode growth is well approximated by that of the maximum Newtonian case, especially as the frequency is increased beyond 5. The deviation of the shear-thinning results from the maximum Newtonian curve in Figure 8b is smaller than that in Figure 7a. Also superimposed on Figures 8a and 8b is the wave growth for the case where the bottom layer does not shear thin at all, that is, $\bar{\eta}_2 = 1$ (labeled *Newtonian Limit* in the figures). Compared with these results, it is seen that the shear-thinning behavior radically destabilizes the system. Next, consider a two-layer system with a shear-thinning bottom layer where now the top layer Newtonian viscosity is lower than the low-strain-rate limiting Newtonian viscosity for the bottom layer. In this case, the viscosity of the shear-thinning layer varies by a factor of approximately 1.5. Figures 9a and 9b give plots of the top and bottom layer growth factors, respectively. In Figure 9b, it is seen that the shear-thinning wave growth behavior closely follows that of the maximum Newtonian curve over a broad frequency range; this is similar to the behavior of these curves seen in Figure 8b, although the agreement here is better. Figure 9c indicates that in contrast to the previous case, the shear-thinning behavior stabilizes the interface mode, compared with a case where no shear thinning occurs at all (the Newtonian limit). In the Newtonian limit, the interface mode is much more unstable than the surface mode (which is typical for large growth situations), and so the shear thinning stabilizes the system (note that results for the Newtonian limit surface mode are not shown).

Consider a two-layer system in which the top layer is shear thinning and the bottom layer is Newtonian. The viscosity varies by approximately a factor of 3 across the top layer. Figures 10a and 10b give plots of the surface and interface mode growth factors, respectively. Note that in contrast with the previous two-layer examples, the minimum and maximum Newtonian cases have the same Newtonian bottom layer viscosity and different top layer viscosities. Figure 10a shows the same trends as in the case where there is a shear-thinning bottom layer, that is, the shear-thinning surface mode results lie between those for the minimum and maximum top layer viscosities. Figure 10b shows that the shear-thinning interface mode growth factors closely follow the curve associated with the minimum Newtonian viscosity in the top layer, that is, the viscosity in the vicinity of the fluid–fluid interface. This is in contrast to previous cases where the bottom layer had shear-thinning and the top layer was Newtonian, and shear-thinning interface mode results followed those curves with the maximum Newtonian viscosity.

Finally, consider a case where both the top and bottom layer have shear thinning. Based on the previous arguments, there are two viscosities that characterize each shear-thinning layer, that is, the minimum and maximum viscosities in each layer. Thus, there are four Newtonian comparisons that can be made with this shear-thinning system. For the purposes of clarity, results are presented for only the interface mode for this shear-thinning case, since this comparison is most transparent. Figure 11 shows interface mode results for the shear-thinning case. Also plotted on this figure are results for a Newtonian system in which the bottom layer has been replaced by its maximum viscosity, and the top layer has been replaced with its minimum viscosity (labeled *Interface* on the plot). Note that the behavior of these two curves is quite similar to those presented previously.

Discussion

The goal of this section is to provide a physical understanding of the effect of shear-thinning behavior on stability results. It is

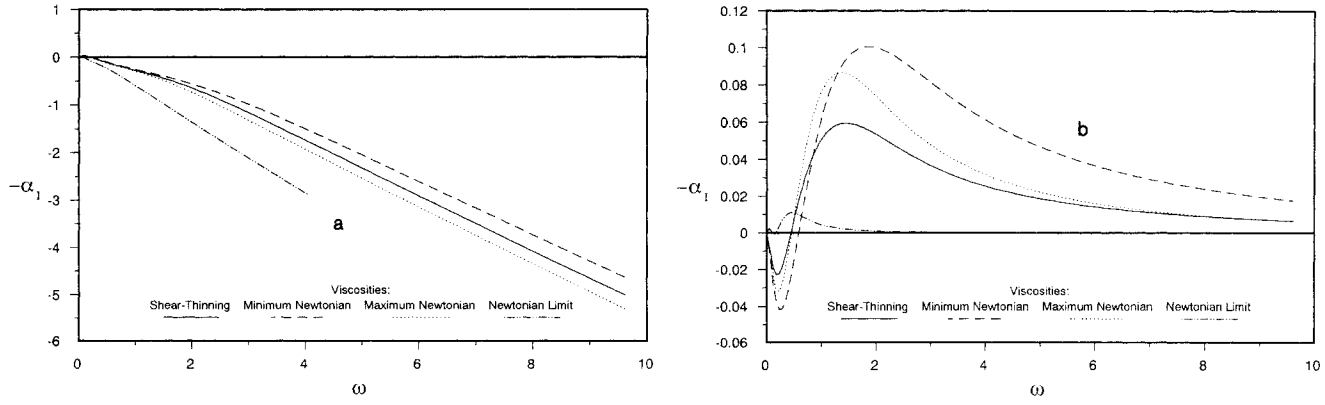

Figure 8. Effect of a shear-thinning bottom layer in a two-layer slide flow.

a. *Surface mode growth factors*

b. *Interface mode growth factors*

Conditions: $\beta = 30°$, $Re = 7.5$, $\overline{Q}_1 = 0.67$, $Ca_1^{-1} = 8.49$
Newtonian top layer with $E_1 = 2$
Bottom layer rheology: $I_2 = 0$, $L_2 = 20.80$, $n_2 = 0.5$
Min. Newtonian viscosity: $\bar{\eta}_{2_{min}} = 0.07113$
Max. Newtonian viscosity: $\bar{\eta}_{2_{max}} = 0.1315$
Also plotted: results where bottom layer does not shear thin (*Newtonian Limit*), $\bar{\eta}_2 = 1$

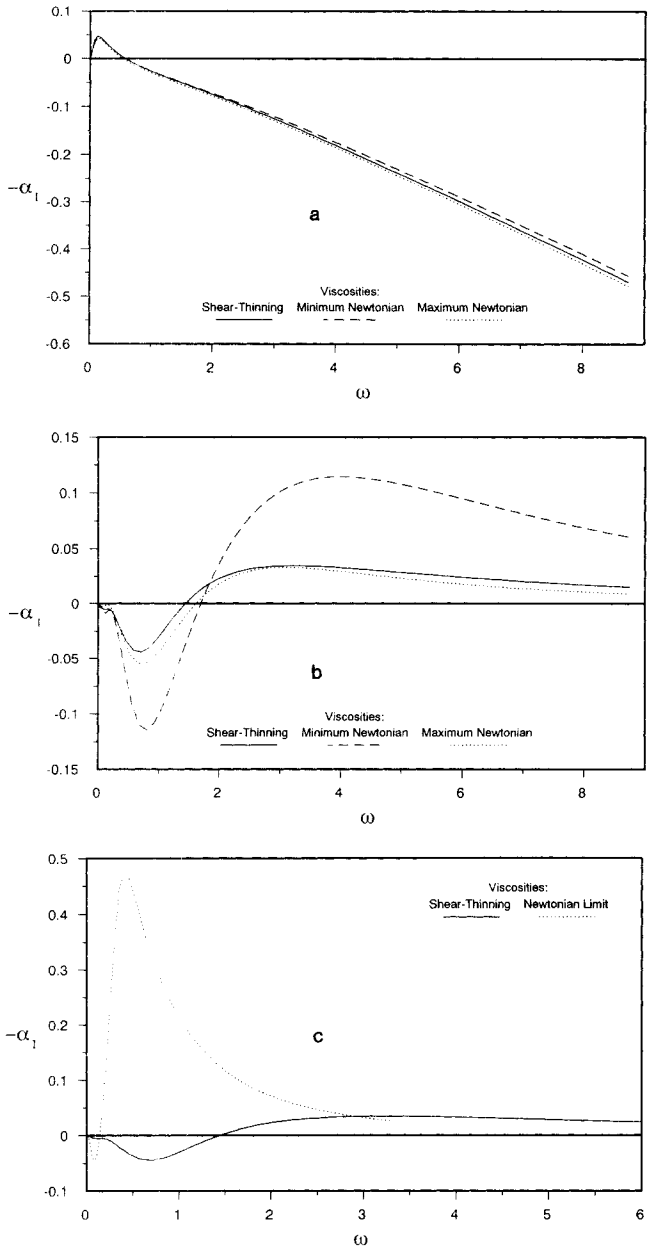

Figure 9. Effect of a shear-thinning bottom layer in a two-layer slide flow.

a. *Surface mode growth factors*

b. *Interface mode growth factors*

Conditions: $\beta = 45°$, $Re = 5.0$, $\overline{Q}_1 = 0.80$, $Ca_1^{-1} = 9.913$
Newtonian top layer with $E_1 = 0.1520$
Bottom layer rheology: $I_2 = 0$, $L_2 = 22.90$, $n_2 = 0.5$
Min. Newtonian viscosity: $\overline{\eta}_{2_{min}} = 0.06730$
Max. Newtonian viscosity: $\overline{\eta}_{2_{max}} = 0.1042$

c. *Comparison of interface wave growth*

Shear-thinning case vs. system where bottom layer does not shear thin at all, $\overline{\eta}_2 = 1$

seen that the shear-thinning behavior affects the interface and surface mode waves in different ways. A mechanism is postulated that accounts for these different behaviors based on energy considerations, making use of work by Kelley et al. (1989) and Hooper and Boyd (1983).

When there is shear thinning, the single-layer wave results of Figures 3 and 4 indicate that except for very small frequencies, the surface mode wave propagates as if it is interacting with an average viscosity of the layer. This is indicated by the fact that the shear-thinning curve lies between the Newtonian results associated with the maximum and minimum viscosities found in the shear-thinning layer. In all the two-layer systems considered, the surface mode waves appear to have the same characteristics as that for the single layer; compare Figures 6, 8a, 9a, and 10a with Figures 3 and 4. The surface mode wave is interacting with an average viscosity associated with the shear-thinning layer, transmitted through the two-layer system. Viewing results in this way further suggests that except at low frequencies, there is no additional non-Newtonian behavior that is affecting the propagation of the surface mode waves beside that due to an average viscosity. This averaging effect is thus due to the global effects of shear thinning, that is, changes in velocity profile, rates of strain, and film thicknesses, Figures 2 and 5.

The interface mode results, however, are quite different from the surface mode results in regard to viewing the effect of shear thinning as an average of the viscosity across a shear-thinning layer. Figure 7a indicates that the growth factors associated with the interface mode do not have values that lie between those associated with the Newtonian results obtained using the minimum and maximum viscosities from the shear-thinning bottom layer. A lower upper bound on the shear-thinning wave growths is given by the maximum Newtonian case (except at small frequencies), where the shear-thinning growth factors are well approximated by those for the maximum Newtonian case as frequencies get larger. These facts suggest that the value of the bottom layer viscosity and the associated strains that are induced in the vicinity of the interface play a large role in determining the propagation characteristics of the interface mode waves; the stability of the interface thus appears to be affected quite strongly by the local viscosity and strain in its vicinity. This is supported by results for Figures 5–7 shown in Table 1, which indicate that the jump in strain across the interface for the shear-thinning system is better approximated by the maximum Newtonian case than the minimum Newtonian case. Note that this is despite the fact that the film thicknesses in the shear-thinning case are better approximated by the minimum Newtonian than the maximum Newtonian case, Figures 5a–5c.

Further evidence for the above postulate is given by Figures 8b and 9b, which show that for cases where the bottom layer exhibits smaller shear thinning (the viscosity varies by less than a factor of 2 in these figures), the shear-thinning results are well approximated by the maximum Newtonian case over a broad frequency range. Again, Table 1 indicates that for these cases the jump in strain across the interface is better approximated by the minimum Newtonian than the maximum Newtonian case. By contrast, Figure 10b indicates that the interface mode shear-thinning results follow the minimum Newtonian data; in this case, there is shear-thinning in the top layer. As indicated by Table 1, the rates of strain in the vicinity of the interface are best approximated by the minimum Newtonian case. The results of the case where both the top and bottom layers have shear thinning, Figure 11, provide further evidence for the role of local viscosity effects in the vicinity of the interface.

A probable explanation for the above results is given in what follows; the arguments presented depend upon some important literature results, which were briefly discussed in the introduc-

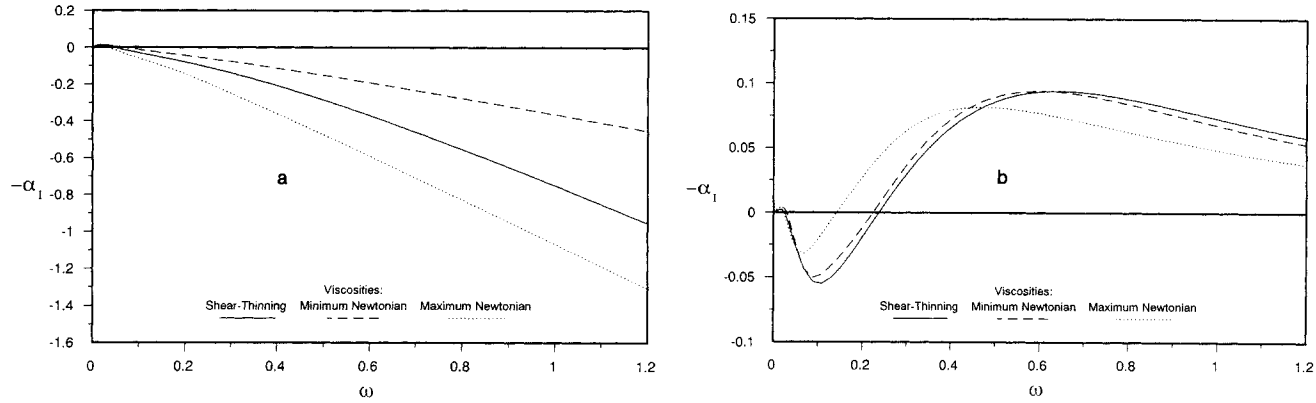

Figure 10. Effect of a shear-thinning top layer in a two-layer slide flow.
a. *Surface mode growth factors*
b. *Interface mode growth factors*
Conditions: $\beta = 15°$, $Re = 65.79$, $\overline{Q}_1 = 0.9$, $Ca_1^{-1} = 30.65$
Newtonian bottom layer
Top layer rheology: $E_1 = 12.47$, $I_1 = 0$, $L_1 = 51.83$, $n_1 = 0.6$
Min. Newtonian viscosity: $\overline{\eta}_{1_{min}} = 3.984$
Max. Newtonian viscosity: $\overline{\eta}_{1_{max}} = 12.47$

tion. By performing an energy balance on a two-layer system undergoing simple shear, Hooper and Boyd (1983) have identified the term responsible for the interfacial instability, which is (with $M_k = 1$):

$$\int (\tilde{V}_{x_2} - \tilde{V}_{x_1})\tilde{\tau}_{xy_2} d\bar{x}|_{\bar{y}=\bar{d}_1} \tag{34}$$

For the purposes of the following arguments, the integration is taken over one wavelength. In general, the difference in the perturbation velocities in the integrand of Eq. 34 is nonzero. This is because the boundary conditions for the linearized problem are applied at the uniform film thickness, $\bar{y} = \bar{d}_1$. Before the linearization is performed, however, the boundary conditions for the governing equations are applied along the wavy interfaces. Thus, it is necessary that the jump in perturbation velocities across the uniform film location (at $\bar{y} = \bar{d}_1$) be nonzero, so that the sum of the uniform film and perturbation velocities will be continuous across the wavy interfaces (to the order of the linear approximation). Physically, then, the integral in Eq. 34 quantifies a transfer in energy from the uniform flow to the linearized problem for the wave propagation.

From similar energy considerations on a single-layer system, Kelly et al. (1989) have determined that the primary term for the instability associated with the free surface is given by:

$$\int (\tilde{V}_{x_1})\tilde{\tau}_{xy_1} d\bar{x}|_{\bar{y}=0} \tag{35}$$

Using the same arguments as those following Eq. 34, the perturbation shear stress at the free surface, $\tilde{\tau}_{xy_1}$, is nonzero; this is so the condition of zero shear can be satisfied at the actual wavy surface for the sum of the uniform film and linearized wave solutions. It is straightforward to show that both Eq. 34 and Eq. 35 arise when considering the two-layer systems presented in this paper (both Newtonian and shear thinning).

Both of the terms, Eqs. 34 and 35, will influence the surface and interface mode solutions. Despite this fact, the similarities between the surface wave instability in the single-layer and two-layer systems suggest that the dominant instability mechanism for the surface mode is associated with Eq. 35, while that for the interface mode is mostly associated with Eq. 34. Using Eq. 19a, it is clear that the integrand of Eq. 34 can be written as:

$$\tilde{\tau}_{xy_2}\tilde{\zeta}_2\left[\frac{d\overline{V}_{x_1}}{d\bar{y}} - \frac{d\overline{V}_{x_2}}{d\bar{y}}\right]\Bigg|_{\bar{y}=\bar{d}_1} \tag{36}$$

In Eq. 36, the bracketed term is the jump in the rate of strain across the interface. Thus, the jump in the rate of strain associated with the uniform flow explicitly appears in the energy term that is responsible for the instability.

As was shown in formulating the stability problem, $\tilde{\tau}_{xy_k}$, $\tilde{\zeta}_k$, and $\tilde{V}_{x_k}$ can all be written in terms of the stream function, where the stream function is a solution to an eigenvalue problem. An

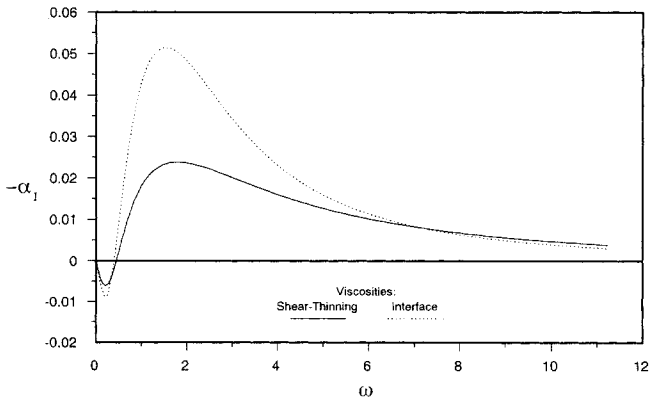

Figure 11. Effect of shear-thinning top and bottom layers on interface mode growth factors in two-layer slide flow.
Conditions: $\beta = 15°$, $Re = 9.00$, $\overline{Q}_1 = 0.50$, $Ca_1^{-1} = 9.37$
Top layer rheology: $E_1 = 2.0$, $I_1 = 0$, $L_1 = 14.25$, $n_1 = 0.6$
Bottom layer rheology: $I_2 = 0$, $L_2 = 28.50$, $n_2 = 0.5$
Interface viscosities: Top layer min. Newtonian viscosity, $\overline{\eta}_{1_{min}} = 1.338$; bottom layer max. Newtonian viscosity, $\overline{\eta}_{2_{max}} = 0.1469$

eigenvalue solution is global in nature since it must satisfy conditions on all the boundaries of the domain; consequently, these terms will exhibit a behavior where shear-thinning effects can be approximated as some average viscosity over the layer in question. To demonstrate that this is indeed the case, the relative sizes of the $\tilde{\tau}_{xy_1}\tilde{V}_{x_1}$ term in Eq. 35 have been evaluated for the shear-thinning, maximum Newtonian, and minimum Newtonian cases of Figure 4. Noting that $\tilde{\tau}_{xy_1}$ and $\tilde{V}_{x_1}$ must be real quantities in the energy term, Eq. 35, a good measure of the size of their product, B, is given by:

$$B = \bar{\gamma}_1 \left| \frac{d^2R_1}{d\bar{y}^2} + \alpha^2 R_1 \right| \left| \frac{dR_1}{d\bar{y}} \right|_{\bar{y}=0} \tag{37}$$

where $||$ denotes the magnitude of the complex argument. Figure 12 gives the results of this comparison, and it is seen that the shear-thinning results lie between those associated with the minimum and maximum Newtonian curves. In addition, note that for all the data presented in this paper, the wavelengths of the shear-thinning, maximum Newtonian, and minimum Newtonian cases are similar, Figures 3b, 6b, and 7b, since the shear-thinning wavelengths appear to be the average of those from the two Newtonian cases. Thus, for all practical purposes the range of integration in Eqs. 34 and 35 for the three cases is similar.

Consequently, it is concluded that a major component of the term in Eq. 36 is due to the local effect of the jump in strain as this jump changes. On the other hand, the expression given by Eq. 35 cannot be simplified so that it has some terms readily identifiable as being of local origin. Furthermore, all the other terms in the energy balance leading to Eqs. 34 and 35 depend solely upon the stream function (Kelly et al., 1989). Based on the above comments made above as to the global nature of $\tilde{\tau}_{xy_2}$ and $\tilde{\zeta}_2$, it is not surprising that the surface mode growth can be interpreted as being due to some average effect over the shear-thinning layer, while the interface mode growth is very dependent on the jump in strain across the interface.

Returning to Figure 7a, it is apparent that in addition to the local effects discussed above, global effects due to shear thinning are important in the growth of interface waves. At higher frequencies, the local effects of viscosity appear to dominate the system stability. However, at frequencies near the largest growth factor [which resides within $\omega \in (2,3)$], global effects due to the shear-thinning eigenfunction solutions appear to play a large role. This manifestation of the global effects is most likely due to inertia. These results are consistent with conclusions drawn by Hooper and Boyd (1983), who provide evidence that in the limit of small wavelength (which corresponds to high frequencies), inertial effects become less important than viscous effects in effecting interfacial instability. As the degree of shear-thinning behavior in the system decreases, however, the global effects of shear-thinning appear to play a smaller role, and the major character of the growth over large frequency ranges appears to be primarily due to the local viscosity effect, Figures 8b, 9b, and 10b.

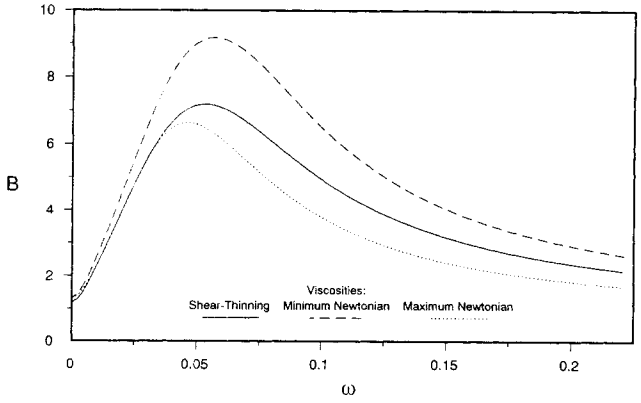

Figure 12. Plot of function B given by Eq. 37 corresponding to single-layer results given in Fig. 4.
Results normalized to $R_1(0)^2$

Finally, it is pointed out that shear-thinning behavior occurring on the inclined plane can be either stabilizing or destabilizing, compared to a case where no shear thinning occurs at all. Comparing the shear-thinning and Newtonian limit cases shown in Figure 8b, it is seen that the shear-thinning case is significantly less stable. Table 1 indicates that the jump in the rate of strain across the interface is significantly smaller than that of the shear-thinning case. Based on the above arguments surrounding Eq. 34, one might qualitatively expect the stability of the Newtonian case to be better than that of the shear-thinning case, where the jump in strain is seen to play such a vital role. On the other hand, Figure 9c shows that the shear-thinning behavior on the inclined plane significantly stabilizes the system compared to one where no shear thinning occurs. As shown in Table 1, the jump in strain across the layers is significantly reduced by the shear-thinning behavior, apparently leading to greater stability.

Conclusions

It has been shown that when there are shear-thinning effects in a multiple-layer system, surface mode waves propagate as if they were in a Newtonian system, where the viscosity is some average of the varying viscosities in the shear-thinning layer. This averaging effect is due to the global effects of shear thinning, such as changes in velocity profile and film thicknesses. On the other hand, waves that are associated with the interfaces between adjacent fluid layers are largely affected by the local viscosity in the vicinity of the interface (and the jump in strain that is thus induced); the propagation is not governed by some average Newtonian viscosity across the layer. Global effects of shear thinning appear to play a role in the growth of these interface waves as well. For two-layer systems, it has also been demonstrated that shear-thinning rheology can either increase or decrease interface wave growth, compared with a Newtonian system in which there is no shear thinning at all. This appears to depend largely on whether the jump in rate of strain across the interface is increased or decreased due to the shear-thinning behavior.

Acknowledgment

The author thanks Kenneth J. Ruschak for guidance and assistance throughout the course of this work, and James Conroy for helping to prepare the figures for this paper.

Notation

A_f = final amplitude
A_i = initial amplitude
B = real product, Eq. 37

Ca_k = capillary number for kth layer, $Ca_k \equiv \eta_{c_n} Q_T / \sigma_k d_s$
d = film thickness
d_s = length scale for thickness of fluid layers
E_k = dimensionless Newtonian viscosity at small rates of strain, $E_k \equiv \eta_{c_k}/\eta_{c_n}$
g = gravitational constant
I_k = dimensionless Newtonian viscosity at large rates of strain, $I_k \equiv \eta_{\infty_k}/\eta_{c_k}$
i = imaginary number
L_k = dimensionless Carreau parameter, $L_k \equiv \delta_k Q_T / d_s^2$
M_k = dimensionless density for kth layer, $M_k \equiv \rho_k/\rho_n$
n = number of fluid layers flowing down incline
n_k = Carreau model parameter for kth layer, analogous to power law exponent
N = number of finite difference points
O = asymptotic order of magnitude
P = pressure
P_a = atmospheric pressure
Q = flow rate per unit width
R = y-dependent part of complex eigenfunction
Re = Reynolds number, $Re \equiv \rho_n Q_T / \eta_{c_n}$
W = length of inclined plane
T = complex amplitude of surface or interlayer wave
t = time
V_x = velocity in x direction
V_y = velocity in y direction
x, y = spatial variables
Y = transformed y value, Eq. 26

Greek letters

α = dimensionless complex wave number
α_I = imaginary part of α, yielding spatial growth information
α_R = real part of α, where $\alpha_R \equiv 2\pi d_s/\lambda$
β = angle of inclination of surface
δ = Carreau model parameter
$\Delta S_{\text{interface}}$ = magnitude of jump in rate of strain across interface, used in Table 1
$\Phi_k(\bar{y})$ = functionality, Eq. 23b
$\dot{\gamma}$ = rate of strain tensor
η = viscosity
η_c = Newtonian viscosity at small rates of strain
η_∞ = Newtonian viscosity at large rates of strain
λ = wavelength
ν = dimensional growth factor
$\Theta_k(\bar{y})$ = functionality, Eq. 23c
$\bar{\theta}_k$ = functionality, Eq. 15f
ρ = density
σ = surface tension
τ = stress tensor
τ_{xx} = component of stress tensor: x momentum transferred in x direction
τ_{xy} = component of stress tensor: x momentum transferred in y direction
ω = dimensionless real frequency
ψ = stream function
ζ = interface location

Subscripts

k = number of layer
n = nth layer
T = total

Additional

$\bar{}$ = dimensionless, uniform film quantities
$\tilde{}$ = dimensionless, small perturbed quantities
$||$ = absolute value; length of complex argument

Literature Cited

Akhtaruzzaman, A. F. M., C. K. Wang, and S. P. Lin, "Wave Motion in Multilayered Liquid Films," *J. Appl. Mech.*, **45**, 25 (1978).

Antrukar, N. R., T. C. Papanastasiou, and J. O. Wilkes, "Stability of Multilayer Extrusion of Viscoelastic Liquids," *AIChE J.*, **36**, 710 (1990).

Benjamin, T. B., "Wave Formation in Laminar Flow Down an Inclined Plane," *J. Fluid Mech.*, **2**, 554 (1957).

Binnie, A. M., "Experiments on the Onset of Wave Formation on a Film of Water Flowing Down a Vertical Plane," *J. Fluid Mech.*, **2**, 551 (1957).

Bird, R. B., R. C. Armstrong, and O. Hassager, *Dynamics of Polymeric Liquids*, **1**, Wiley, New York (1977).

Hooper, A. P., and W. G. Boyd, "Shear-Flow Instability at the Interface between Two Viscous Fluids," *J. Fluid Mech.*, **23**, 507 (1983).

Kao, T. W., "Stability of Two-Layer Stratified Flow Down an Inclined Plane," *Phys. Fluids*, **8**(5), 812 (1965a).

———, "Role of the Interface in the Stability of Stratified Flow Down an Inclined Plane," *Phys. Fluids*, **8**(12), 2190 (1965b).

———, "Role of Viscosity Stratification in the Stability of Two-Layer Flow Down an Inclined Plane," *J. Fluid Mech.*, **33**, 561 (1968).

Kelly, R. E., D. A. Goussis, S. P. Lin, and F. K. Hsu, "The Mechanism for Surface Wave Instability in Film Flow Down an Inclined Plane," *Phys. Fluids*, **1**(5), 819 (1989).

Lin, S. P., "Stability of a Non-Newtonian Liquid Film Flowing Down an Inclined Plane," *Phys. Fluids*, **10**(1), 69 (1967).

Loewenherz, D. S., and C. J. Lawrence, "The Effect of Viscosity Stratification on the Stability of a Free Surface Flow at Low Reynolds Number," *Phys. Fluids*, **1**(10), 1686 (1989).

Shaqfeh, E. S. G., R. G. Larson, and G. H. Fredrickson, "The Stability of Gravity-Driven Viscoelastic Film Flow at Low to Moderate Reynolds Number," *J. Non-Newt. Fluid Mech.*, **31**, 87 (1989).

Wang, C. K., J. J. Seaborg, and S. P. Lin, "Instability of Multilayered Liquid Films," *Phys. Fluids*, **21**(10), 1669 (1978).

Waters, N. D., "The Stability of Two Stratified 'Power-Law' Liquids in Couette Flow," *J. Non-Newt. Fluid Mech.*, **12**, 85 (1983).

Waters, N. D., and A. M. Keeley, "The Stability of Two Stratified Non-Newtonian Liquids in Couette Flow," *J. Non-Newt. Fluid Mech.*, **24**, 161 (1987).

Yih, C., "Stability of Liquid Flow Down an Inclined Plane," *Phys. Fluids*, **6**(3), 321 (1963).

———, "Stability of a Non-Newtonian Liquid Film Flowing Down an Inclined Plane," *Phys. Fluids*, **8**(7), 1257 (1965).

Appendix: Derivation of Asymptotic Results

In this appendix, the asymptotic results given by Eqs. 29 are derived. For a single layer, Eqs. 6, 9, 10, and 12 become:

$$\bar{\tau}_{xy} = -\bar{y} \tag{A1a}$$

$$\bar{\tau}_{xy} = \bar{\eta} \frac{d\bar{V}_x}{d\bar{y}} \tag{A1b}$$

$$\bar{\eta} = I + (1 - I)\left[1 + \left(L \frac{d\bar{V}_x}{d\bar{y}}\right)^2\right]^{(n-1)/2} \tag{A1c}$$

$$\bar{V}_x = 0 \quad \text{at } \bar{y} = \bar{d} \tag{A1d}$$

$$1 = \int_0^{\bar{d}} \bar{V}_x d\bar{y} \tag{A1e}$$

In the above equations, all subscripts denoting the single layer have been dropped for clarity. Equations A1 constitute a well-posed problem to determine the velocity field and the film thickness. An asymptotic solution to the above system is to be obtained in the limit of small non-Newtonian behavior, where the velocity and dimensionless film thicknesses are perturbed as in Eqs. A2. (Note that in this appendix, subscripts 0 and 2 denote the order of the terms in the asymptotic expansions.)

$$\bar{V}_x \sim \bar{V}_{x_0}[\bar{y}; I, n] + L^2 \bar{V}_{x_2}[\bar{y}; I, n] + O(L^4) \quad \text{as } L \to 0 \tag{A2a}$$

$$\bar{d} \sim \bar{d}_0[I, n] + L^2\bar{d}_2[I, n] + O(L^4) \quad \text{as } L \to 0 \quad \text{(A2b)}$$

These expansions are substituted into Eqs. A1, and terms of like orders in L are collected. The lowest order problem to be solved is:

$$\frac{d\bar{V}_{x_0}}{d\bar{y}} = -\bar{y}$$

$$\bar{V}_{x_0} = 0 \quad \text{at } \bar{y} = \bar{d}_0$$

$$1 = \int_0^{\bar{d}_0} \bar{V}_{x_0} d\bar{y}$$

The solution to this problem is:

$$\bar{V}_{x_0} = 1/2\,(\bar{d}_0^2 - \bar{y}^2) \quad \text{(A3a)}$$

$$\bar{d}_0 = \sqrt[3]{3} \quad \text{(A3b)}$$

The next order problem consisting of terms to $O(L^2)$ is given by:

$$\frac{d\bar{V}_{x_2}}{d\bar{y}} = \frac{1}{2}(1 - n)(1 - I)\left(\frac{d\bar{V}_{x_0}}{d\bar{y}}\right)^3$$

$$\bar{V}_{x_2} = \bar{d}_0\bar{d}_2 \quad \text{at } \bar{y} = \bar{d}_0$$

$$0 = \int_0^{\bar{d}_0} \bar{V}_{x_2} d\bar{y}$$

The solution is:

$$\bar{V}_{x_2} = 1/8\,(1 - n)(1 - I)(\bar{d}_0^4 - \bar{y}^4) + \bar{d}_0\bar{d}_2 \quad \text{(A4a)}$$

$$\bar{d}_2 = -3/10\,(1 - n)(1 - I) \quad \text{(A4b)}$$

The results, Eqs. A3 and A4, coupled with the expansions, Eqs. A2, yield Eqs. 29.

Manuscript received June 13, 1990, and revision received Oct. 1, 1990.